An Integrated Phosphoproteomics Work Flow Reveals Extensive Network Regulation in Early Lysophosphatidic Acid Signaling*[S]

Thiemo B. Schreiber‡, Nina Mäusbacher‡, György Kéri§¶, Jürgen Cox‖, and Henrik Daub‡**

Lysophosphatidic acid (LPA) induces a variety of cellular signaling pathways through the activation of its cognate G protein-coupled receptors. To investigate early LPA responses and assess the contribution of epidermal growth factor (EGF) receptor transactivation in LPA signaling, we performed phosphoproteomics analyses of both total cell lysate and protein kinase-enriched fractions as complementary strategies to monitor phosphorylation changes in A498 kidney carcinoma cells. Our integrated work flow enabled the identification and quantification of more than 5,300 phosphorylation sites of which 224 were consistently regulated by LPA. In addition to induced phosphorylation events, we also obtained evidence for early dephosphorylation reactions due to rapid phosphatase regulation upon LPA treatment. Phosphorylation changes induced by direct heparin-binding EGF-like growth factor-mediated EGF receptor activation were typically weaker and only detected on a subset of LPA-regulated sites, indicating signal integration among EGF receptor transactivation and other LPA-triggered pathways. Our results reveal rapid phosphoregulation of many proteins not yet implicated in G protein-coupled receptor signaling and point to various additional mechanisms by which LPA might regulate cell survival and migration as well as gene transcription on the molecular level. Moreover, our phosphoproteomics analysis of both total lysate and kinase-enriched fractions provided highly complementary parts of the LPA-regulated signaling network and thus represents a useful and generic strategy toward comprehensive signaling studies on a system-wide level. ***Molecular & Cellular Proteomics 9:1047–1062, 2010.***

Lysophosphatidic acid (LPA)[1] is a simple bioactive lipid that activates G protein-coupled receptors (GPCRs) and elicits a variety of biological responses, such as cell proliferation, migration, and survival (1, 2). In addition to important physiological functions in, for example, vascular biology and wound healing, LPA signaling has also been implicated in pathophysiological processes, such as the onset and progression of human cancers (3, 4). The lipid mediator LPA is primarily generated upon extracellular hydrolysis of larger lysophospholipids by the secreted enzyme autotaxin, a lysophospholipase D that is up-regulated in several cancers and was initially identified as an autocrine motility factor for tumor cells (5). To date, seven high affinity receptors for LPA (LPA_{1-5}, GPR 87, and P2Y5) are known with distinct but overlapping expression patterns. The well characterized LPA receptors LPA_{1-3}, which belong to the endothelial differentiation gene family of lysophospholipid-recognizing GPCRs, activate multiple signaling pathways through heterotrimeric G proteins from the G_i, G_q, and $G_{12/13}$ families (2, 6). Activation of G_i inhibits adenylyl cyclase-mediated production of cyclic AMP and has been implicated in the activation of the ERK and phosphatidylinositol 3-kinase signaling (1, 2). LPA also triggers G_q-dependent signals through phospholipase C-mediated generation of the second messengers diacylglycerol and inositol 1,4,5-trisphosphate, which induce protein kinase C

From the ‡Cell Signaling Group, Department of Molecular Biology and ‖Department of Proteomics and Signal Transduction, Max Planck Institute of Biochemistry, Am Klopferspitz 18, 82152 Martinsried, Germany, §Vichem Chemie Ltd., Herman Ottó u. 15, Budapest 1022, Hungary, and ¶Pathobiochemistry Research Group of the Hungarian Academy of Science, Semmelweis University, Puskin u. 9, Budapest 1088, Hungary

Received, October 16, 2009, and in revised form, November 19, 2009

Published, MCP Papers in Press, January 12, 2010, DOI 10.1074/mcp.M900486-MCP200

[1] The abbreviations used are: LPA, lysophosphatidic acid; GPCR, G protein-coupled receptor; EGF, epidermal growth factor; HB-EGF, heparin-binding EGF-like growth factor; ERK, extracellular-signal regulated kinase; PKD, protein kinase D; EGFR, epidermal growth factor receptor; MAPK, mitogen-activated protein kinase; ADAM, a disintegrin and metalloproteinase; SILAC, stable isotope labeling by amino acids in cell culture; LDS, lithium dodecyl sulfate; Bis-Tris, 2-[bis(2-hydroxyethyl)amino]-2-(hydroxymethyl)propane-1,3-diol; SCX, strong cation exchange; nano-LC, nanoscale capillary LC; LTQ, linear trap quadrupole; IPI, International Protein Index; GO, gene ontology; DAVID, Database for Annotation, Visualization and Integrated Discovery; STRING, Search Tool for the Retrieval of Interacting Genes/Proteins; AAK1, AP2-associated protein kinase 1; FAK, focal adhesion kinase; MAP, mitogen-activated protein; GAP, GTPase-activating protein; GRLF1, glucocorticoid receptor DNA-binding factor 1; ARHGAP29, Rho GTPase-activating protein 29; GEF, guanine nucleotide exchange factor; PEA15, phosphoprotein enriched in astrocytes 15; PDCD4, programmed cell death protein 4; HDAC, histone deacetylase; BMPR2, bone morphogenic protein receptor 2; DHCR7, 7-dehydrocholesterol reductase.

activity and elevate cytosolic calcium levels (2, 7). Moreover, LPA induces rapid cytoskeletal rearrangements, such as stress fiber formation via $G_{12/13}$-mediated activation of the small GTPase Rho (7–9). Early LPA signaling can cooperatively regulate downstream effectors as for example demonstrated for the convergence of G_i-, G_q-, and $G_{12/13}$-triggered pathways on protein kinase D (PKD) (7, 10).

In many cell types, LPA stimulation leads to the rapid transactivation of the epidermal growth factor receptor (EGFR) receptor tyrosine kinase, which relays mitogenic downstream signaling through ERK MAPK- and Akt/protein kinase B-dependent pathways (4, 7, 11–13). This GPCR-EGFR cross-talk is mediated by ADAMs, which proteolytically cleave transmembrane precursors to generate mature EGFR ligands, such as heparin-binding EGF-like growth factor (HB-EGF) or amphiregulin (13–17). The GPCR-induced mechanisms underlying cellular metalloproteinase regulation are still incompletely understood. Potential control elements include G_i and G_q (18, 19), Src family and phosphatidylinositol 3-kinases (20, 21), and Rac and Ras GTPase effector pathways.

Taken together, extensive previous research unveiled LPA as a rapid inducer of multiple pathways that form interdependent networks and utilize protein kinases and phosphorylation-based signaling to drive key biological processes, such as cell proliferation, survival, and migration. However, as previous studies have not analyzed LPA-triggered kinase signaling in an unbiased manner, it is unclear to what extent our current knowledge is still incomplete.

Notably, recent developments in mass spectrometry-based proteomics have set the stage for global approaches toward GPCR-mediated signaling to address these issues. In particular, stable isotope labeling by amino acids in cell culture (SILAC) (22), optimized phosphopeptide fractionation and enrichment protocols (23, 24), high resolution MS on ion trap/orbitrap hybrid instruments (25), and breakthroughs in MS data processing (26) can now be integrated in efficient phosphoproteomics work flows to quantify thousands of phosphorylation events in a cellular system. Furthermore, new enrichment techniques based on affinity purification with immobilized inhibitors provide a valuable tool to selectively increase the analytical sensitivity for protein kinases, which are often underrepresented in total cell lysate analysis because of their low cellular abundance (27–29). The detection of regulated phosphorylation events on protein kinases can be particularly informative as these enzymes are located at critical nodes of signaling cascades and networks.

Here, we applied SILAC-based, quantitative phosphoproteomics in a differential analysis of phosphorylation events triggered by either LPA or HB-EGF stimulation. To assess the overall contribution of EGFR transactivation to early phosphorylation changes upon LPA treatment, human A498 kidney carcinoma cells were used as a cancer-relevant cell line in which LPA rapidly elicits EGFR-dependent signaling by ADAM-mediated processing of pro-HB-EGF ligand precursors (13). Our quantitative analysis revealed numerous new phosphorylation events that are likely associated with either known biological responses or point to previously unrecognized signaling elements in the context of LPA-triggered GPCR signaling. In this study, we further demonstrate that parallel phosphoproteomics of total cell lysate and kinase-enriched fractions provides highly complementary sets of data and therefore represents a general strategy to assess phosphorylation-based signaling networks in a comprehensive manner.

EXPERIMENTAL PROCEDURES

Cell Culture and Cell Lysis—A498 cells were cultured in Dulbecco's modified Eagle's medium (Invitrogen) supplemented with 10% fetal bovine serum (Invitrogen), glutamine, non-essential amino acids, and sodium pyruvate. For SILAC, cells were grown for 8 days in Dulbecco's modified Eagle's medium containing either normal L-arginine (Arg0) at 42 mg/liter and L-lysine (Lys0) at 71 mg/liter or equimolar amounts of L-[U-$^{13}C_6$,$^{14}N_4$]arginine (Arg6) and L-[$^2H_4$]lysine (Lys4) or L-[U-$^{13}C_6$,$^{15}N_4$]arginine (Arg10) and L-[U-$^{13}C_6$,$^{15}N_2$]lysine (Lys8) (from Sigma Isotec or Cambridge Isotope Laboratories). Cells were serum-starved for 2 days prior to growth factor stimulation. In the first experiment, Arg0/Lys0-labeled cells were left untreated, Arg6/Lys4-labeled cells were stimulated with 0.5 ng/ml HB-EGF (Sigma-Aldrich) for 3 min, and Arg10/Lys8-labeled cells were treated with 10 μM LPA (Sigma-Aldrich or Biomol) for 3 min. In the second experiment, Arg0/Lys0-labeled cells were stimulated with LPA, Arg6/Lys4-labeled cells were left untreated, and Arg10/Lys8-labeled cells were stimulated with HB-EGF. For each condition, labeled cells from 35 dishes (15-cm diameter) were lysed with ice-cold lysis buffer containing 50 mM HEPES-NaOH, pH 7.5, 150 mM NaCl, 0.5% Triton X-100, 1 mM EDTA, 1 mM EGTA, 10 μg/ml aprotinin, 10 μg/ml leupeptin, 1 mM PMSF, 10 mM NaF, 2.5 mM Na_3VO_4, 50 ng/ml calyculin A, 1% phosphatase inhibitor mixture 1 (Sigma), and 1% phosphatase inhibitor mixture 2 (Sigma) for 5 min on ice. Lysates were precleared by centrifugation at 16,500 $\times$ *g* at 4 °C for 30 min and subsequently filtered through a 0.45-μm PVDF membrane. Protein concentrations were determined by the BCA assay (Pierce), and lysates were pooled at equal protein amounts. Stimulation was controlled by immunoblot analysis with phosphoepitope-specific antibody recognizing Tyr(P)^{1173} of the EGF receptor (Cell Signaling Technology, Inc.). Aliquots of 15 mg of pooled total cell lysate were lyophilized and stored at −80 °C, whereas the large remainders were subjected to kinase affinity enrichment.

Kinase Affinity Resins and Enrichment—The kinase inhibitors VI16832, AX14596, and SU6668 were prepared as described elsewhere (27, 30, 31). VI16741 was synthesized as VI16832 except that 8-ethyl-2-methanesulfonyl-8*H*-pyrido[2,3-*d*]pyrimidin-7-one was used as starting material instead of 8-bicyclo-[2.2.1]hept-2-yl-2-methanesulfonyl-8*H*-pyrido[2,3-*d*]pyrimidin-7-one. Commercially available inhibitors were bisindolylmaleimide X (Alexis Biochemicals), purvalanol B (Tocris), and dasatinib (LC Laboratories). For immobilization, 2 volumes of 5 mM bisindolylmaleimide X, 10 mM AX14596, 1.5 mM VI16832, 5 mM VI16741, or 5 mM dasatinib were coupled to 1 volume of drained epoxy-activated Sepharose 6B beads (GE Healthcare) according to a reported protocol (30). To generate purvalanol B and SU6668 resins, 2 volumes of 10 mM inhibitor solutions prepared in 50% *N*,*N*-dimethylformamide, 50% EtOH were mixed with 1 volume of drained EAH-Sepharose 4B (GE Healthcare) and then subjected to carbodiimide-catalyzed immobilization according to described procedures (28). The combined total protein extract (270 and 405 mg of protein in experiments 1 and 2, respectively) was adjusted

to 1 M NaCl and incubated for 3 h at 4 °C on a rotating wheel with 2.5 ml of inhibitor resin mixture consisting of 500 μl of VI16832 beads, 500 μl of purvalanol B beads, 300 μl of SU6668 beads, 300 μl of bisindolylmaleimide X beads, 300 μl of dasatinib beads, 300 μl of AX14596 beads, and 300 μl of VI16741 beads. Afterward, the mixed resin beads were washed twice with 50 ml of buffer containing 50 mM HEPES-NaOH, pH 7.5, 1 M NaCl, 0.25% Triton X-100, 1 mM EDTA, 1 mM EGTA, 10 mM NaF, and 0.1 mM Na_3VO_4; once with 50 ml of a similar buffer containing 150 mM instead of 1 M NaCl; and once with 50 ml of 50 mM HEPES-NaOH, 10 mM NaF, 0.1 mM Na_3VO_4. Bound proteins were eluted five times at 60 °C with 3 ml of 0.5% SDS, 5 mM DTT. Elution fractions were lyophilized and stored at −80 °C until further processing.

MS Sample Preparation and Phosphopeptide Enrichment—Kinase-enriched fractions were dissolved in water, combined, and precipitated (28). 70% of the protein precipitate was resolved by gel electrophoresis followed by in-gel digestion, whereas the remaining 30% was digested in solution. For in-gel digestion, pellets were dissolved in 1.5× LDS buffer and separated by LDS-PAGE using NuPAGE Novex 4–12% Bis-Tris gels (Invitrogen) according to the manufacturer's instructions. The gels were stained with the Colloidal Blue Staining kit (Invitrogen) and cut into 14 slices. The slices were subjected to in-gel digestion with trypsin as described elsewhere (32). After the final concentration step, 10% of the resulting peptide fractions were adjusted to 2% TFA and desalted on doubly packed, homemade C_{18} StageTips (33). The remainders were pooled for peptide fractions from adjacent slices, and phosphopeptides were enriched from the resulting seven fractions. For trypsin digestion in solution, 30% of the kinase-enriched precipitates were dissolved in 7 M urea, 2 M thiourea, 50 mM HEPES-NaOH, pH 7.5; reduced, alkylated, and sequentially digested with Lys-C (Wako) and modified trypsin (sequencing grade; Promega) at an enzyme/substrate ratio of 1:100 as described (24) prior to phosphopeptide enrichment.

For phosphoproteome analysis in total cell extracts, 5 mg of lysate per treatment condition were pooled, lyophilized, dissolved in water, and then precipitated (28). Precipitated proteins were proteolytically digested as described above at an enzyme/substrate ratio of 1:200. Peptides were diluted to a final volume of 10 ml in 30% ACN, 0.2% TFA and separated by strong cation chromatography with a 1-ml Resource S column (GE Healthcare) on an ÄKTA Explorer System as described (24). Bound peptides were eluted with a gradient from 100% buffer A (5 mM KH_2PO_4, 30% ACN, 0.01% TFA) to 30% buffer B (5 mM KH_2PO_4, 30% ACN, 0.01% TFA, 350 mM KCl) followed by phosphopeptide enrichment from the column flow-through and the SCX elution fractions.

For phosphopeptide purification, 5 mg of TiO_2 beads (GL Sciences Inc.) were washed once with elution buffer (NH_3 water in 20% ACN, pH 10.5) and equilibrated with washing buffer (50% ACN, 0.1% TFA). TiO_2 beads were loaded with dihydroxybenzoic acid by incubation with loading buffer (6 g/liter dihydroxybenzoic acid in 15% ACN). Peptide samples were adjusted to a final concentration of 30% ACN, 2 M urea, 0.5 M thiourea and incubated with TiO_2 beads for 60 min at room temperature on a rotating wheel. Subsequently, beads were washed three times with washing buffer, and bound phosphopeptides were eluted for 10 min at room temperature with elution buffer containing 20% ACN followed by a second elution step with buffer containing 40% ACN. In the case of the in-solution digested, kinase-enriched fraction and the SCX flow-through of the total lysate sample, supernatants were repeatedly applied to fresh TiO_2 beads to obtain four distinct elution fractions from consecutive TiO_2 resin incubations. All eluates were filtered through homemade C_8 StageTips. The eluates were concentrated in a vacuum concentrator (Eppendorf). Before MS analysis, samples were adjusted to 1% ACN and 0.05% TFA.

MS Analysis—Tryptic peptides were separated by on-line reverse phase nanoscale capillary LC (nano-LC; Agilent 1100) coupled to ESI-MS/MS. Using the nano-LC system, samples were injected onto a 15-cm reverse phase, fused silica capillary column (inner diameter, 75 μm; packed in-house with 3-μm ReproSil-Pur C_{18}-AQ medium; Dr. Maisch GmbH) kept at 31 °C. The nano-LC system was connected to an LTQ-Orbitrap mass spectrometer (Thermo Fisher Scientific) equipped with a nanoelectrospray ion source (Proxeon Biosystems). Loaded peptides were eluted with 140-min gradients ranging from 5 to 40% ACN in 0.5% acetic acid with a flow rate of 250 nl/min. Data-dependent acquisition was performed on the LTQ-Orbitrap using the Xcalibur 2.0 software in the positive ion mode as described (27). Briefly, the instrument was recalibrated in real time by co-injection of an internal standard from ambient air into the C-trap ("lock mass option") (25). Survey spectra were acquired in the orbitrap with a resolution of 60,000 at *m/z* 400. Up to five of the most intense multiply charged ions were sequentially isolated, fragmented, and analyzed in the LTQ part of the instrument. To improve phosphopeptide analysis, multistage activation was enabled, and the neutral loss species at 97.97, 48.99, or 32.66 *m/z* below the precursor ion were activated for 30 ms during fragmentation (pseudo-MS^3) (34). All raw data files from this study have been uploaded to the Tranche file-sharing system (https://proteomecommons.org/, hash 4n6ku2WlUvPMeWBPJnvyijMR0KcaGWOOF6QGasC2CPSVf1-JA3AfuX1cSrOVd3DYNZoJiD8erLQsKLR6GLfTzalZYPuIAAAAAAAAA-98g==).

MS Data Processing—Raw MS data were processed using the in-house software MaxQuant (version 1.0.12.16) (26). MaxQuant-generated peak lists were searched with the Mascot search engine (version 2.2.04; Matrix Science, London, UK) against an in-house curated International Protein Index (IPI) human protein database (version 3.37 containing 69,141 entries) and 175 commonly observed contaminants (such as human keratins, porcine trypsin, and endoproteinase Lys-C) to which reversed versions of all sequences had been added. The maximum mass deviations allowed for MS and MS^2 peaks were 5 ppm and 0.5 Da, respectively. Carbamidomethylcysteine was set as fixed modification, and oxidized methionine, phosphorylation on serine, threonine, or tyrosine and protein *N*-acetylation were searched as variable modifications. In addition, the SILAC labels Lys4, Lys8, Arg6, and Arg10 were searched as modifications. Full tryptic specificity was required, and up to three missed cleavages were allowed. Searches against a concatenated target/decoy database allowed us to filter peptide and protein identifications for a false discovery rate of less than 1% (35).

Identified peptides were automatically quantified, and phosphorylation sites assigned by post-translational modification score-based localization in MaxQuant (24, 26). For phosphorylation site analysis, only class I sites with a localization probability of at least 0.75 and a localization probability score difference of 5 or higher were considered (24). For identified class I sites, annotated phosphopeptide spectra have been uploaded to the Tranche file-sharing system (https://proteomecommons.org/, hash: m2s2DEyBC5mrrGzsYh-5obIbEC94X2SgIfnb0Y7gCoBqhmmnv0QH9tFv0EjRvh0YnYyEhkT-U3o7sT7oKmEE8Sa0KudUQAAAAAAA8ixg==). All phosphopeptide ratios were normalized for unequal protein amounts and $\log_2$-transformed. In the case of singly and multiply phosphorylated peptides harboring the same site, ratios were separately calculated for singly, doubly, and multiply phosphorylated species to detect possible priming phosphorylation events. To identify significantly regulated phosphopeptides on the basis of biological reproducibility, the ratios of the individual peptide ratios determined in the two experiments were calculated. Gaussian regression analysis on the histogram plot of the $\log_2$-transformed ratios of ratios was performed using Sigmaplot (version 10.0; Systat Software Inc.). The obtained values

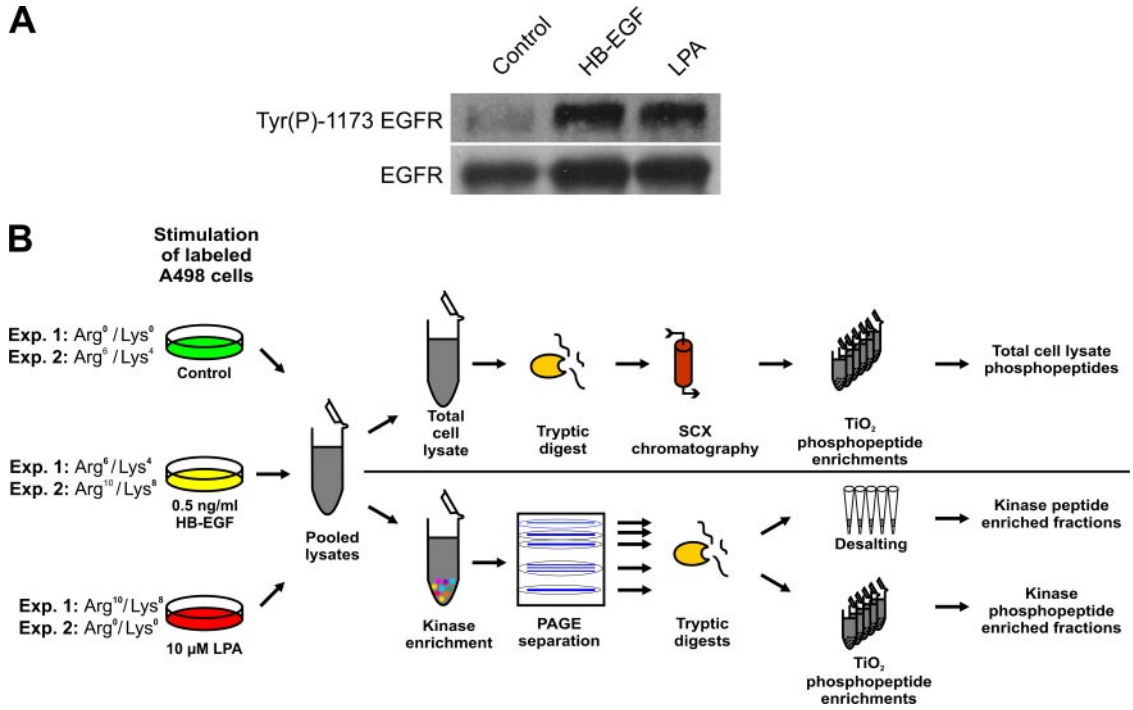

FIG. 1. **Stimulation conditions and experimental design.** *A*, LPA- and HB-EGF-induced tyrosine phosphorylation of the EGFR in SILAC-encoded A498 cells. Immunoblot analysis of total cell extracts with antibody recognizing Tyr(P)^{1173} in the EGFR revealed similar stimulation upon treatment with either 0.5 ng/ml HB-EGF or 10 μM LPA. EGFR levels were similar as verified by immunoblotting with anti-EGFR antibody. *B*, schematic illustration of the integrated proteomics work flow for quantitative phosphorylation analysis of total lysates and kinase-enriched fractions. *pY*, phosphotyrosine.

for the mean and S.D. across the whole quantitative data set were used to determine thresholds for significant regulation of at least ± 2.5 σ. Furthermore, only phosphosites conforming to this criterion and showing consistent regulation in biological replicates were considered as regulated for further analysis.

Gene Ontology (GO) and STRING Network Analyses—Significantly overrepresented GO terms were identified with the DAVID gene functional classification tool (36). To identify significant enrichment of GO terms, the Expression Analysis Systematic Explorer (EASE) score threshold in DAVID was set to $p \leq 0.05$. Kinase-enriched fractions were analyzed for overrepresented GO molecular function terms using the complete human proteome as the background data set. To analyze regulated phosphoproteins from total cell lysate experiments for enrichment of GO biological process terms, all identified phosphoproteins were used as reference data.

All proteins with confidently identified LPA-regulated phosphorylation sites were uploaded to the STRING protein-protein interaction database (37). The interaction network was generated on the basis of experimental and database knowledge with seven external interactors and visualized with Cytoscape (38).

RESULTS

Integrated Work Flow for Comprehensive Signaling Analysis—The GPCR ligand LPA rapidly triggers phosphorylation-dependent signaling in many mammalian cell types. In addition to capturing these changes in A498 kidney cancer cells on a proteome-wide level, our goal was to compare EGFR transactivation in the context of GPCR signaling with a similar activation of the EGFR by exogenous ligand. Therefore, we initially monitored time- and dose-dependent EGFR autophosphorylation at Tyr(P)^{1173} upon addition of HB-EGF to define which concentration induced EGFR activation similar to that observed upon LPA-induced processing of endogenous HB-EGF precursors (supplemental Fig. 1). These test experiments revealed that 10 μM LPA or 0.5 ng/ml HB-EGF induced comparable EGFR Tyr(P)^{1173} phosphorylation, which peaked after 3 min of stimulation. Thus, these treatment conditions were deemed as suitable for further SILAC-based proteomics analyses (Fig. 1*A*). To enable quantitative comparisons, populations of A498 cells were differentially labeled with three combinations of isotopic lysine and arginine variants (Lys0/Arg0, Lys4/Arg6, and Lys8/Arg10) as indicated in Fig. 1*B*. After five cell doublings in SILAC media to ensure near complete incorporation into cellular proteomes, A498 cells were stimulated with growth factors and lysed, and equal protein amounts of total cell extract were pooled. Furthermore, we performed two independent experiments with different labeling schemes to assess the reproducibility and reliability of SILAC-based quantifications in biological replicates.

Total cellular protein extracts were digested with trypsin, and the resulting peptide mixture was resolved by SCX chromatography into eight fractions followed by phosphopeptide enrichment with TiO_2 beads. As the TiO_2 resin only captured a fraction of the phosphopeptides present in the initial flow-through of the SCX column, the supernatant was consecu-

TABLE I
Comparison of biological replicate analyses

Experiment	Uniquely modified phosphopeptides	Phosphorylated proteins	Phosphorylated protein kinases
Only in experiment 1	1,947	242	25
Overlap	1,967	1,081	168
Only in experiment 2	3,902	746	26

TABLE II
Comparison of results from kinase-enriched fractions and total cell lysates

Fraction	Uniquely modified phosphopeptides	Phosphorylated proteins	Phosphorylated protein kinases
Only in kinase enrichment	1,898	273	73
Overlap	516	445	107
Only in total cell lysate	5,402	1,351	39

tively applied to further phosphopeptide enrichment steps to capture remaining phosphopeptide species. All phosphopeptide fractions were analyzed by LC-MS on an LTQ-Orbitrap mass spectrometer.

In addition, we enriched for protein kinases to enable their analysis with considerably higher sensitivity than achievable from total cell extracts. Protein kinases are often difficult to detect in total phosphoproteomes because of their relatively low expression compared with their more abundant substrates. However, as kinases represent the key elements of phosphorylation-based signal transmission, knowledge about their site-specific phosphorylations can provide important insights into the architecture of signaling networks and their regulation by external stimuli. We therefore incubated total cell extract with a mixture of seven kinase inhibitor resins with distinct binding characteristics to enable the affinity purification of a maximum number of kinases from A498 cells. After extensive washing, 70% of the kinase-enriched fraction was resolved by gel electrophoresis prior to in-gel digestions with trypsin followed by phosphopeptide enrichment. We further prepared total peptide fractions from gel slices to monitor whether protein changes occur in kinase-enriched fractions upon growth factor treatment. The remaining 30% of the inhibitor resin eluate was digested in solution and subjected to consecutive enrichments with TiO_2 beads as a complementary strategy for phosphopeptide fractionation. All resulting peptide fractions were analyzed on an LTQ-Orbitrap mass spectrometer. An overview of our phosphoproteomics strategy for the parallel analysis of both total cell lysate and kinase-enriched fractions is shown in Fig. 1*B*. All raw MS data from two independent experiments were collectively processed using the MaxQuant software package, which automatically performed peptide to protein assignment, SILAC-based quantification of proteins and phosphorylation events, and phosphorylation site localization in identified phosphopeptides (26).

Qualitative and Quantitative Phosphoproteomics Analysis of A498 Cells—The combined analysis of kinase-enriched and total lysate fractions led to the identification of 3,914 and 5,869 distinct phosphopeptides (supplemental Table 1) in the first and second biological replicate experiments, respectively (Table I), with an overlap of 1,967 phosphopeptides detected in both experiments. In total, the identified phosphopeptides were derived from 2,115 distinct proteins (supplemental Table 2), and 5,332 class I phosphorylation sites (supplemental Table 3) could be assigned with high confidence ($p \geq 0.75$).

Moreover, of the 2,414 distinct phosphopeptides detected upon kinase enrichment, only 516 were found among the 5,918 phosphopeptides identified from total cell lysates (Table II). Thus, the two phosphoproteomics strategies yield highly complementary data sets, and this was also evident on the level of identified protein kinases. Notably, 73 of the 219 distinct protein kinases identified with phosphopeptides were only found upon prefractionation. The estimated kinome coverage of the inhibitor resin mixture was about 70% based on our data that 107 of the 146 phosphorylated protein kinases identified from total cell lysates were also found in the affinity-purified fractions. Moreover, our analysis of total peptide fractions upon kinase enrichment revealed an additional 43 kinases identified exclusively with non-phosphorylated peptides. In total, as many as 262 distinct protein kinases according to nomenclature by Manning *et al.* (39) were detected; this to the best of our knowledge, represents the highest number of these key enzymes identified from a single biological source to date. The overall relative abundances of Ser(P), Thr(P), and Tyr(P) were 88.9, 10.3, and 0.8% in total lysate and 69.2, 22.1, and 8.7% in kinase-enriched fractions, consistent with a higher prevalence of Tyr(P) on protein kinases reported earlier (27). We further used GO analysis to identify significantly overrepresented molecular functions in the identified phosphoproteins. As expected, protein kinase activity was highly overrepresented upon kinase prefractionation (supplemental Fig. 2 and Table 4).

Quantification was possible for about 97% of the more than 29,000 uniquely modified peptides (supplemental Table 1) identified in this study. Overall, identified peptides harbored 5,155 or 5,169 distinct class I ($p \geq 0.75$) phosphorylation sites

for which quantitative data could be obtained upon either LPA or HB-EGF treatment, respectively. For statistical analysis, measured ratios were $\log_2$-transformed and normalized on all measured peptide ratios. To determine the interexperimental variance and define threshold values for significantly regulated sites, corresponding normalized phosphopeptide ratios from both experiments were divided by each other to calculate "ratios of ratios." After binning and plotting a histogram chart, the mean and σ of the ratio distribution were determined by Gaussian fourth order regression (Fig. 2, *A* and *B*). Based on this analysis, we applied stringent filter criteria to our data set and considered only sites for further analysis if they were consistently up- or down-regulated by more than 2.5 times σ in both experiments (Fig. 2*C* and supplemental Table 5).

As cells were stimulated with either LPA or HB-EGF for only 3 min before lysis, protein changes were highly unlikely to occur within this short treatment period. Therefore, we only analyzed phosphopeptide-enriched fractions from total lysate. However, as it cannot be formally excluded that rapidly induced post-translational modifications might affect inhibitor binding of some kinases, we also analyzed total peptide fractions upon kinase enrichment in addition to phosphopeptide fractions. Notably, none of the identified phosphoproteins exhibited stimulation-dependent binding. Consequently, the ratios of regulated phosphorylations were highly similar with or without normalization for protein abundance (Fig. 2*D*). Because of this high concordance, we did not normalize these phosphorylation changes for protein levels. This further ensured consistency of phosphorylation data from kinase-enriched fractions with our results from total lysate phosphoproteome analysis, which we considered as important for further bioinformatics processing of merged data sets.

In total, about 5% of all quantified phosphorylation sites were significantly and reproducibly regulated upon growth factor treatment. LPA stimulation led to significant and reproducible changes at 224 confidently assigned phosphorylation sites (supplemental Table 6) of which 150 were up-regulated and 74 were down-regulated. By comparison, with only 23 phosphorylation sites up-regulated and 21 down-regulated, HB-EGF treatment resulted in a considerably smaller number of phosphorylation changes (Fig. 4 and supplemental Table 6). Notably, 43 of all regulated sites have not been identified previously according to the phosphorylation site database PhosphoSitePlus®. Selected phosphorylation sites are compiled in Table III.

LPA-triggered Dephosphorylation Events—Although the majority of phosphorylations were induced upon treatment, we found down-regulation for a considerable number of sites. This raises the question whether these signaling events could be due to rapid, growth factor-induced dephosphorylation. In the case of a dephosphorylation event, the relative abundance of the non-phosphorylated counterpart of a phosphopeptide would increase to an extent determined by the change in phosphorylation site stoichiometry. Remarkably, we could identify a small number of dephosphorylation events based on such observations, for example for a peptide derived from the protein-tyrosine kinase Abl. The peptide ^{574}GQGESDPLDHEPAVpSPLLPR^{593}, which encompasses Ser(P)^{588}, was reduced upon LPA stimulation by a factor of 2.5, whereas a more than 3-fold up-regulation was observed for its unphosphorylated counterpart (Fig. 3*A*). Similarly, dephosphorylation events were also detected on a multiply phosphorylated peptide of the AP2-associated protein kinase 1 (AAK1) encompassing Ser(P)^{676} and Ser(P)^{678} as evident from a decrease of phosphorylated species accompanied by a 4-fold increase of the non-phosphorylated counterpart. To our knowledge, these results provide the first experimental evidence of early dephosphorylation events in LPA signaling.

Alternative to dephosphorylation, the phosphorylation site ratio determined from a singly phosphorylated peptide species can decrease in the case of an induced secondary phosphorylation mapping to the same peptide as illustrated by a set of peptides harboring the adjacent phosphorylation sites Ser(P)^{205} and Ser(P)^{208} from the serine/threonine PKD1 (Fig. 3*B*). In response to LPA, both the unphosphorylated and the Ser^{205} phosphorylated peptide species were down-regulated by about 2-fold, whereas the corresponding singly and doubly phosphorylated Ser(P)^{208}-containing peptides exhibited reciprocal ratios. These results demonstrate LPA-induced phosphorylation on Ser^{208} of PKD1 and further suggest that phosphorylation on Ser^{205} did neither change nor prime phosphoryl transfer on the adjacent serine residue. Notably, phosphorylation on Ser^{205} and Ser^{208} has been implicated in the molecular association of PKD1 with 14-3-3β in response to oxidative stress (40) and might therefore have regulatory functions in the context of LPA-triggered signaling.

Comparison of Phosphorylation Changes upon LPA and HB-EGF Treatment—In our experiments, we used an HB-EGF concentration titrated to induce similar EGFR phosphorylation on Tyr(P)^{1173} as triggered by the LPA-induced transactivation process. This was also evident from the MS-based quantification of EGFR Tyr(P)^{1110}, which was identified in one of the two replicate experiments and quantified with ratios of 2.5 and 1.9 upon HB-EGF and LPA incubation, respectively. HB-EGF induced fewer phosphorylation changes than LPA as expected because of the LPA-selective activation of Rho GTPase and other GPCR-triggered signaling pathways. Furthermore, nearly all HB-EGF-regulated phosphorylation sites exhibited regulation in the same direction upon LPA in concordance with the EGFR transactivation component of LPA signaling. The only exceptions were found for Ser(P)^{548} of PKD1, which was 4.6-fold induced by LPA in contrast to a 5.7-fold down-regulation upon HB-EGF treatment, and for the Ser(P) residues 4476, 4485, and 4489 on plectin-1, which were found to be significantly reduced by HB-EGF but not by LPA treatment. In contrast, the majority of all other HB-EGF-

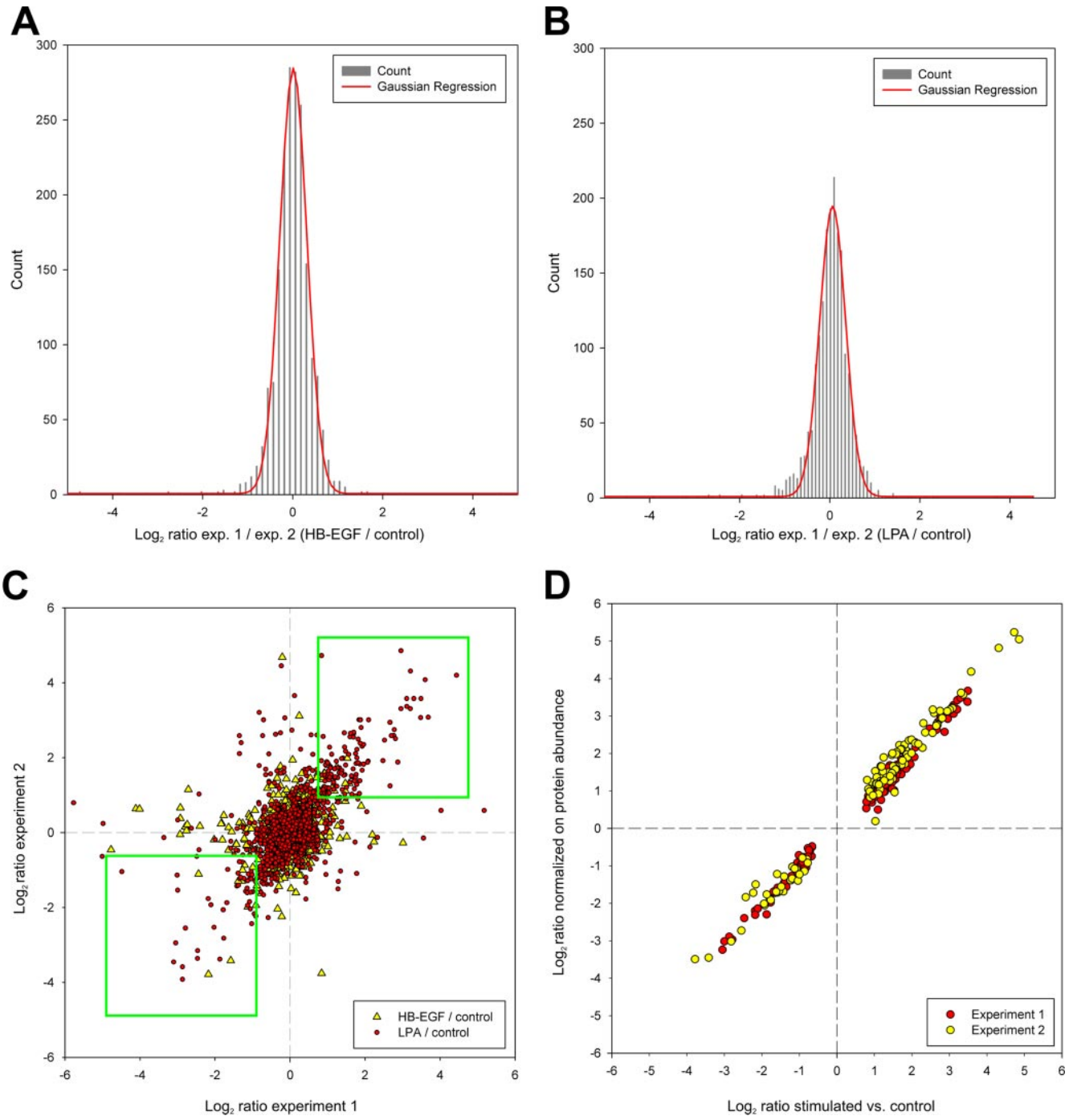

FIG. 2. **Statistical and comparative analyses of quantitative MS data.** Quantified phosphopeptides were binned according to their $\log_2$ values of the ratio of their HB-EGF (*A*) or LPA (*B*) *versus* control ratios obtained in biological replicates. Gaussian regression analysis was applied to calculate the mean and S.D. for the $\log_2$-transformed ratios of ratios. *C*, correlation of phosphorylation site ratios upon HB-EGF or LPA treatment shown in a scatter plot comparison of biological replicates. Consistently up- and down-regulated sites *enclosed* by either of the two *rectangles* were considered for further analysis. *D*, regulated phosphosite ratios determined from kinase-enriched fractions were similar with or without normalization for protein abundance as visualized by a scatter plot.

regulated sites showed more pronounced changes upon LPA treatment despite similar EGFR activation (Fig. 4).

Bioinformatics Analysis of LPA-induced Phosphoproteome Changes—Next, we performed a GO analysis to identify significantly overrepresented biological process categories in the subset of LPA-regulated phosphoproteins using all identified proteins with phosphorylation sites as the background data set (supplemental Table 7). We found LPA-regulated phos-

TABLE III

Selected LPA-regulated phosphorylation sites

Remarks were deduced from GO and Kyoto Encyclopedia of Genes and Genomes (KEGG) annotations or directly from the literature where indicated. Ratios only measured in one experiment are indicated by asterisks.

Protein	IPI	Position	Sequence window	Mean Ratio HB-EGF/Control	Mean Ratio LPA/Control	Remarks
Receptors						
Bone morphogenetic protein receptor type-2	IPI00783156	757	LPKRPT***S***LPLNTK	1.32	2.60	
Epidermal growth factor receptor	IPI00018274	1166	KGSHQI***S***LDNPDY	1.13	1.86	
Epidermal growth factor receptor	IPI00018274	1110	SVQNPV***Y***HNQPLN	3.12*	1.95*	Autophosphorylation site
Ephrin type-B receptor 2	IPI00252979	586	KLQHYT***S***GHMTPG	2.83	10.33	
Hepatocyte growth factor receptor	IPI00029273	977	YDARVH***T***PHLDRL	0.63	0.44	
Non-receptor kinases / phosphatases						
Proto-oncogene tyrosine-protein kinase ABL1	IPI00221171	16	GDQRRP***S***LPALHF	0.96	2.14	Novel site
Proto-oncogene tyrosine-protein kinase ABL1	IPI00221171	588	DHEPAV***S***PLLPRK	0.86	0.40	
Tyrosine-protein kinase ABL2	IPI00329488	820	RTVSTS***S***QPEENV	1.14	2.50	
Focal adhesion kinase 1	IPI00413961	386	EKQGMR***T***HAVSVS	1.40	2.64	Activation loop
Focal adhesion kinase 1	IPI00413961	577	MEDSTY***Y***KASKGK	1.40	2.08	
Serine/threonine-protein kinase D3	IPI00015538	731	RIIGEK***S***FRRSVV	2.08	13.55	Activation loop
Serine/threonine-protein kinase D3	IPI00015538	735	EKSFRR***S***VVGTPA	2.31	6.77	Activation loop
Protein tyrosine kinase 2 beta	IPI00029702	579	YIEDED***Y***YKASVT	3.39	15.03	Activation loop
Protein tyrosine kinase 2 beta	IPI00029702	580	IEDEDY***Y***KASVTR	2.22	8.75	Activation loop
Protein tyrosine kinase 2 beta	IPI00029702	583	EDYYKA***S***VTRLPI	2.45	9.58	Activation loop
Ribosomal protein S6 kinase alpha-1	IPI00017305	573	ENGLLM***T***PCYTAN	1.25	3.03	Activation loop
Tyrosine-protein kinase Tec	IPI00000878	519	YVLDDQ***Y***TSSSGA	1.63	6.99	Phosphorylation activates enzyme (62)
Proto-oncogene tyrosine-protein kinase Yes	IPI00013981	425	LIEDNE***Y***TARQGA	1.21	1.84	Activation loop
Cyclin-dependent kinase-like 5	IPI00746301	407	NIPHLL***S***PKEAKS	1.58	2.91	
Tyrosine-protein phosphatase non-receptor type 12	IPI00289082	435	KLERNL***S***FEIKKV	2.02	2.89	Protein tyrosine phosphatase
Tyrosine-protein phosphatase non-receptor type 12	IPI00018914	578	RPRPAT***S***TPDLAS	0.82	0.49	Protein tyrosine phosphatase
Cell cycle / Apoptosis						
Serine/threonine-protein kinase Chk1	IPI00023664	280	KRPRVT***S***GGVSES	1.52	2.09	Involved in G2/M transition
Astrocytic phosphoprotein PEA-15	IPI00643342	116	DIIRQP***S***EEEIIK	1.17	2.03	Site stabilizes anti-apoptotic effect (42-43)
STE20-like serine/threonine-protein kinase	IPI00247439	340	PASKRA***S***SDLSIA	1.10	2.17	Implicated in the regulation of apoptosis (63)
Serine/threonine-protein kinase 17B	IPI00014934	10	RRFDCR***S***ISGLLT	1.58	5.89	Implicated in the regulation of apoptosis
Endo- / Exocytosis						
AP2-associated protein kinase 1	IPI00479760	620	QKVGSL***T***PPSSPK	1.54	2.86	Endocytosis
AP2-associated protein kinase 1	IPI00479760	623	GSLTPP***S***SPKTQR	1.23	3.50	Endocytosis
AP2-associated protein kinase 1	IPI00479760	624	SLTPPS***S***PKTQRA	1.51	2.80	Endocytosis
AP2-associated protein kinase 1	IPI00479760	637	GHRRIL***S***DVTHSA	0.68	0.43	Endocytosis
AP2-associated protein kinase 1	IPI00479760	676	SATTTP***S***GSPRTS	0.49	0.17	Endocytosis
AP2-associated protein kinase 1	IPI00479760	731	PEKLGG***S***AESLIP	0.92	0.33	Endocytosis
AP-2 complex subunit beta-1	IPI00784366	4	___MTD***S***KYFTTN	2.73	8.40	Endocytosis
GTPase-activating protein and VPS9 domain-containing protein 1	IPI00292753	929	RLVRSR***S***SDIVSS	1.23	1.90	Endocytosis
Dynamin-1	IPI00413140	774	VPAGRR***S***PTSSPT	1.38	2.55	Endocytosis, downstream of EGFR (20)
Dynamin-1	IPI00413140	776	AGRRSP***T***SSPTPQ	1.47	2.47	Endocytosis, downstream of EGFR
Exocyst complex component 1	IPI00215762	486	MGNMSA***S***DLDVAD	0.55	0.58	Exocytosis, CDC42 interactor (64)
Kinesin-like protein KIF21A	IPI00425409	855	TRKLSS***S***DAPAQD	0.58	3.74	Intracellular transport
Intersectin-1	IPI00304740	904	ATGSSP***S***PVLGQG	0.29	0.46	Endocytosis, Rho signalling

TABLE III—*continued*

G protein signaling						
Guanine nucleotide-binding protein subunit alpha-12	IPI00328744	40	REARRR***S***RDIDAL	0.88*	3.13*	Heterotrimeric G protein α subunit
Glucocorticoid receptor DNA-binding factor 1	IPI00334715	589	DRNQKN***S***LSDPNI	1.68	2.75	Rho GAP, represses glucocorticoid receptor
A-kinase anchor protein 13	IPI00065931	1899	IFANRR***S***QQSVSL	1.62	3.55	Rho GEF, couples Gα12/13 to Rho, anchors PKA
Rho GTPase-activating protein 29	IPI00152011	499	GFGPAN***S***LEDVVR	0.96	2.61	Ras/Rho GAP, Rho/CDC42 regulation
Rho GTPase-activating protein 29	IPI00152011	552	GSSESR***S***LDSESI	1.26	2.44	Ras/Rho GAP, Rho/CDC42 regulation
Cdc42 effector protein 4	IPI00015894	174	GAAGPH***S***PDPLLD	0.53	3.71	Effector of CDC42, pseudopodium formation
Development and differentiation-enhancing factor 1	IPI00376976	1044	AIQKQA***S***EDSNDL	1.08	2.54	Regulation of Ras/Arf GTPase activity
Ras-related protein Rab-13	IPI00016373	178	KSGGRR***S***GNGNKP	1.34	3.25	GTPase activity
TBC1 domain family member 4	IPI00220901	588	MRGRLG***S***VDSFER	1.22	2.80	Ras/Rab GTPase activity
Neurofibromin	IPI00299512	2543	LLGTRK***S***FDHLIS	1.49	3.56	Ras GTPase activator
Neurofibromin	IPI00299512	2515	PTVGQT***S***PRARKS	0.67	0.27	Ras GTPase activator
Rab GTPase-binding effector protein 1	IPI00293009	407	GLRRAQ***S***TDSLGT	0.74	0.40	Rab effector, GTPase activator activity
Protein SOLO	IPI00748767	961	HLGEEA***S***PRGYRR	1.02	0.52	Rho GEF activity, GTPase regulator activity
MICAL-like protein 1	IPI00174962	484	PAPRAP***S***ASPLAL	0.34	0.09	Rab 13 interactor
Transcription / translation / degradation						
Programmed cell death protein 4	IPI00290110	457	GRKRFV***S***EGDGGR	1.60	1.83	Site de-represses AP-1 elements (45)
Transcription elongation factor B polypeptide 3	IPI00018404	137	KKHRKL***S***ELERPH	1.44	3.64	Elongation factor
Nuclear factor 1 X-type	IPI00218260	265	VTLGRR***S***ITSPPS	1.57	3.25	Transcription factor
Histone deacetylase 7	IPI00418482	486	PLSRAQ***S***SPAAPA	1.45	1.97	Histone deacetylation, site triggers nuclear export
Histone deacetylase 7	IPI00418482	444	RLRQIP***S***AEDLET	0.81*	3.42*	Histone deacetylation
Gem-associated protein 5	IPI00291783	757	TPVKLE***S***IDGNEE	1.30	3.69	EIF4H interactor (65)
Eukaryotic translation initiation factor 4H	IPI00014263	21	FGGGRG***S***RGSAGG	1.21	2.22	Translation initiation factor
Ubiquitin conjugation factor E4 B	IPI00005715	103	SQSLSR***S***QSMDID	1.14	1.90	Protein degradation
Ubiquitin-associated protein 2-like	IPI00514856	454	APPPPS***S***PLPSKS	0.81	0.49	Protein degradation
Ubiquitin-associated protein 2-like	IPI00514856	609	PSSISS***S***PQKDLT	0.93	0.48	Protein degradation
DNA damage response						
Interferon-inducible double stranded RNA-dependent protein kinase activator A	IPI00021167	18	PLERED***S***GTFSLG	1.76	4.66	Protein activates interferon-inducible double stranded RNA-dependent protein kinase
Adhesion / motility						
CD44 antigen	IPI00305064	697	VEDRKP***S***GLNGEA	1.31	3.03	Site regulates motility (58)
Platelet F11 receptor	IPI00001754	284	VIYSQP***S***ARSEGE	2.47	5.69	Cell adhesion
Tight junction protein ZO-1	IPI00216219	1366	SYFDRR***S***FENKPP	1.39	2.86	Adherens junction
Plakophilin-3	IPI00335634	88	QSSSPV***Y***GSSAKT	1.65	2.20	Cell adhesion
Plakophilin-3	IPI00026952	314	TLQRLS***S***GFDDID	2.62	18.39	Cell adhesion
Liprin-beta-1	IPI00179172	532	NLDRKR***S***ASAPTL	1.87	3.67	Cell adhesion
Myristoylated alanine-rich C-kinase substrate	IPI00219301	120	AEPGSP***T***AAEGEA	0.85	2.23	Phosphorylation inhibits F-actin binding
Other Proteins						
ADAM 9	IPI00288894	791	SSTAAK***S***FEDLTD	0.81*	0.53*	Involved in ligand shedding
ADAM 17	IPI00440932	752	PSRQPG***S***VPRHVS	2.05*	3.72*	Involved in ligand shedding
C-X-C chemokine receptor type 4	IPI00216445	328	TSVSRG***S***SLKILS	0.76*	3.43*	Receptor for stromal derived factor-1
7-dehydrocholesterol reductase	IPI00294501	14	NIPKAK***S***LDGVTN	1.25	7.70	Cholesterol synthesis, activated by phosphorylation (54)
Oxysterol-binding protein-related protein 11	IPI00032970	189	ISQRRP***S***QNAISF	1.10	1.95	Sterol transport/sensing (66)
1-phosphatidylinositol-4,5-bisphosphate phosphodiesterase	IPI00010400	537	SLEPQK***S***LGDEGL	2.68	14.32	Phospholipase

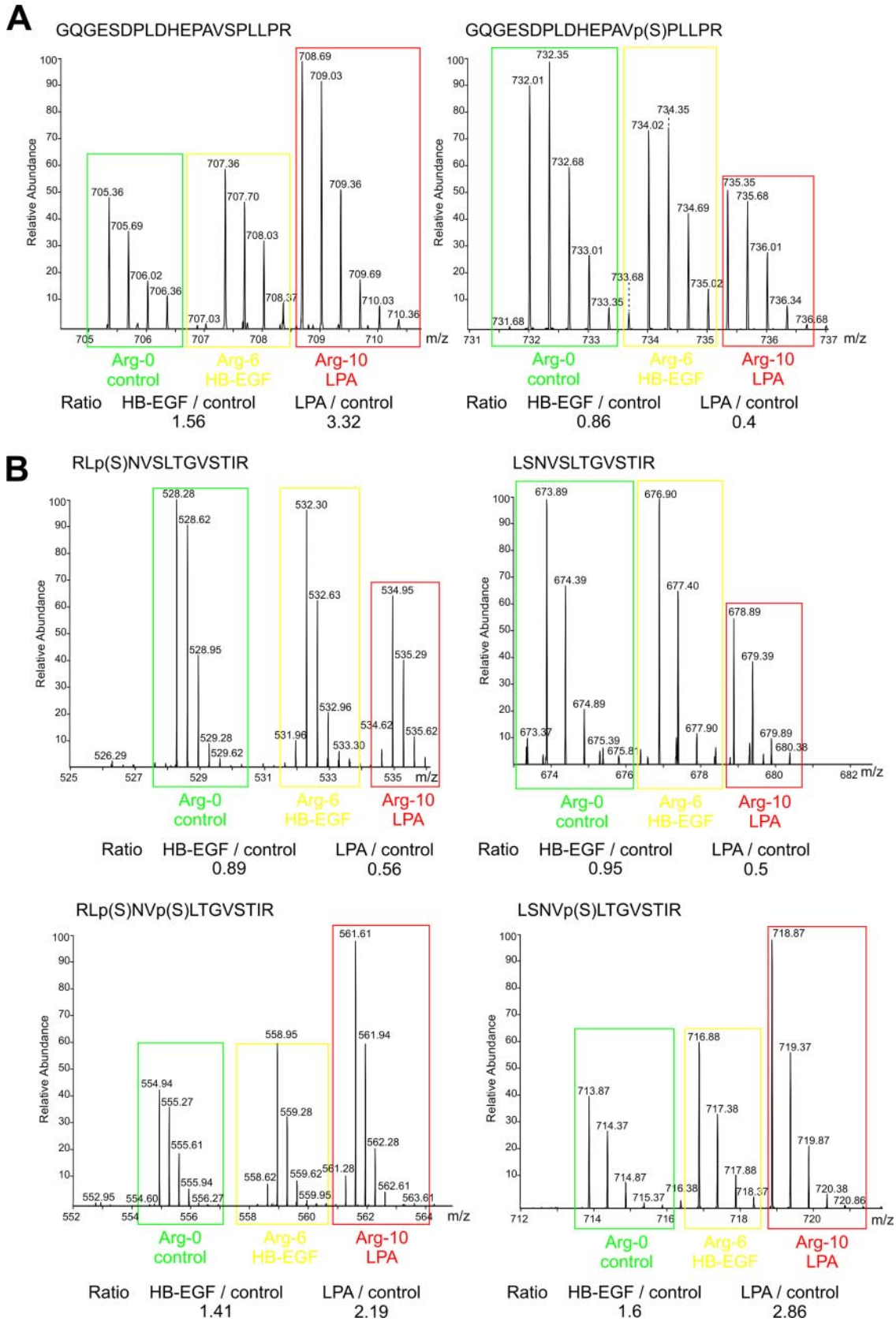
A
GQGESDPLDHEPAVSPLLPR
Relative Abundance
m/z
Arg-0 control
Arg-6 HB-EGF
Arg-10 LPA
Ratio HB-EGF / control 1.56
LPA / control 3.32
GQGESDPLDHEPAVp(S)PLLPR
Ratio HB-EGF / control 0.86
LPA / control 0.4
B
RLp(S)NVSLTGVSTIR
Ratio HB-EGF / control 0.89
LPA / control 0.56
LSNVSLTGVSTIR
Ratio HB-EGF / control 0.95
LPA / control 0.5
RLp(S)NVp(S)LTGVSTIR
Ratio HB-EGF / control 1.41
LPA / control 2.19
LSNVp(S)LTGVSTIR
Ratio HB-EGF / control 1.6
LPA / control 2.86

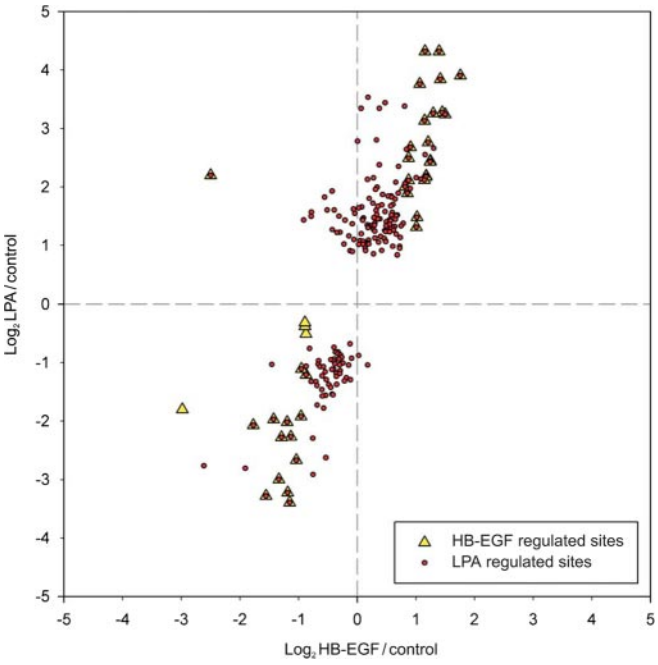

FIG. 4. **Differential phosphorylation changes upon treatment with LPA and HB-EGF.** A scatter plot analysis of phosphorylation sites significantly and reproducibly changed upon LPA (●) or HB-EGF (▲) treatment in both experiments is shown. Values on the *x axis* (*y axis*) correspond to $\log_2$-transformed average phosphorylation ratios determined upon HB-EGF (LPA) stimulation of A498 cells.

phoproteins enriched for proteins annotated to biological processes, such as cell proliferation, cell motility, and cell adhesion with highest enrichment found in the latter category (Fig. 5). To further analyze the functional relationships among LPA signaling components, we queried the STRING database to assemble a protein-protein interaction network based on the regulated phosphoproteins identified in this study (Fig. 6). We solely considered associations backed up by experimental data and allowed for a few external interactors to enhance network connectivity. Network analysis revealed multiple interactions between central kinase mediators of LPA signaling, such as the EGFR, focal adhesion kinase (FAK), and ERK MAP kinases, and LPA-regulated phosphoproteins implicated in migration and adhesion, such as CD44, paxillin, the myristoylated alanine-rich protein kinase C substrate MARCKS, F11 receptor, and the protein-tyrosine phosphatase PTPN12. Tyrosine phosphorylations of FAK and paxillin are well characterized signaling events upon LPA-induced activation of the small GTPase Rho, and the protein network further illustrates various interactions among regulators and effectors of Rho GTPases, such as the GTPase-activating proteins (GAPs) glucocorticoid receptor DNA-binding factor 1 (GRLF1) and Rho GTPase-activating protein 29 (ARHGAP29) as well as the guanine nucleotide exchange factor (GEF) protein kinase A anchor protein 13. Additionally, LPA regulated site-specific phosphorylations on the GEF SOLO and the Cdc42 effector protein 4 (41). The heterotrimeric G protein subunit $G\alpha_{12}$ couples $LPA_{1/2}$ receptors to Rho GTPase activation, and we could identify an LPA-induced phosphorylation site in one experiment. Collectively, our results indicate that LPA-triggered kinase activities modulate Rho GTPase signaling on multiple levels and suggest complex mechanisms of signal integration instead of linear signal transduction processes. The network analysis of LPA-modulated phosphoproteins further revealed that the RhoGTPase GAPs GRLF1 and ARHGAP29 are connected to the endocytosis regulators intersectin 1 (ITSN1) and dynamin 1 (DNM1). In addition to modulation of Rho GTPase signaling, our quantitative MS analysis identified LPA regulation of components involved in signaling through Ras, Rab, and Arf small GTPases, such as development and differentiation enhancing factor 1, neurofibromin, TBC1 domain family member 4, and others.

A major signaling response to LPA involves the phosphorylation and activation of the protein kinase Akt/protein kinase B (14). Although Akt does not bind to our kinase enrichment resin and was therefore not detected in our MS analyses, we added this known mediator in LPA signaling to gain better insights into cellular network regulation. Notably, this provided additional links involving the known Akt substrates phosphoprotein enriched in astrocytes 15 (PEA15) and the protein kinase Chk1 for which we detected LPA-induced phosphorylation on their known Akt substrate sites. Phosphorylation of PEA15 on Ser^{116} is known to exert site-specific, antiapoptotic effects by protein stabilization (42, 43), and thus our identification of this site in LPA signaling points to a mechanism potentially involved in the antiapoptotic actions of the GPCR ligand. Chk1 is a serine/threonine kinase involved in the control of S phase and G_2/M phase checkpoint during the cell cycle and is activated upon various types of DNA damage. Interestingly, Akt prevents this activation by phosphorylating Chk1 on Ser^{280}, the site that we found up-regulated upon LPA in our present study (44). This indicates a potential mechanism by which LPA-induced GPCR signaling could modulate the DNA damage response.

Remarkably, our data indicate potential mechanisms for rapid regulation of transcriptional activity upon LPA treatment.

FIG. 3. **MS spectra from SILAC-based quantitative analysis.** *A*, MS spectra of peptides derived from the tyrosine kinase Abl. The peptide with the amino acid sequence GQGESDPLDHEPAVSPLLPR was quantified in its non-phosphorylated and singly phosphorylated form harboring $Ser(P)^{588}$. *B*, MS spectra of a set of peptides derived from the serine/threonine kinase PKD1. Peptides harboring the phosphorylation sites on Ser^{205} and Ser^{208} were quantified as non-, singly, or doubly phosphorylated forms with either phosphorylation detected in distinct singly modified peptide variants. *A* and *B*, isotopic variants originated from the differentially labeled and stimulated cells as indicated. Ratios obtained by SILAC-based quantification are shown. *p(S)*, phosphoserine.

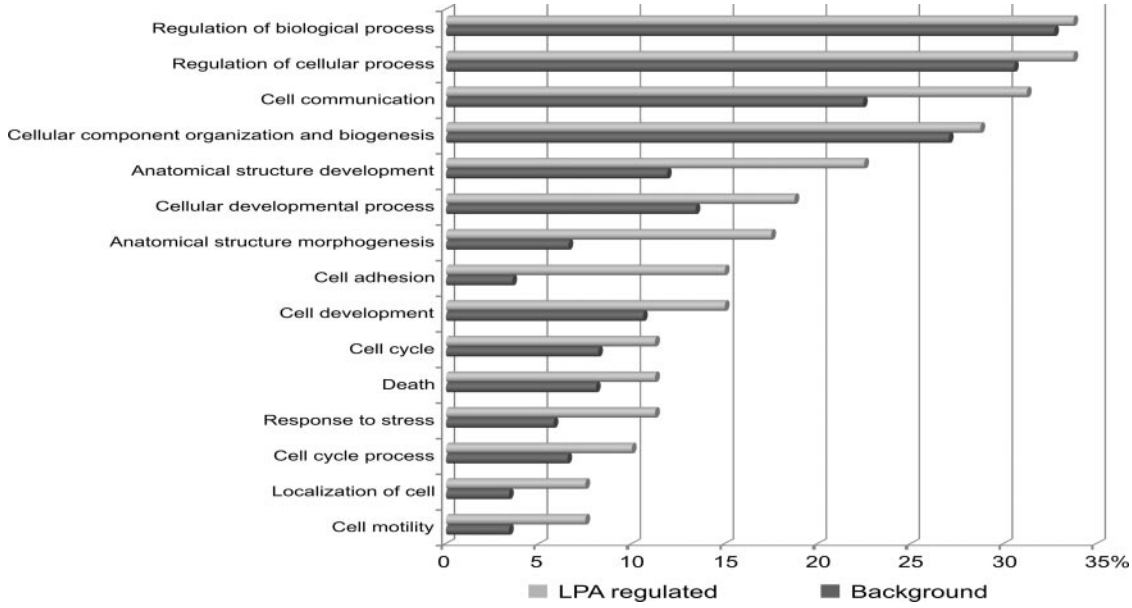

FIG. 5. **Overrepresented GO biological process categories.** LPA-regulated phosphoproteins from total cell lysate were compared with all phosphoproteins identified in the total cell lysate. Significantly overrepresented GO biological process terms ($p < 0.05$) are shown. Percentage values indicate the fractions of proteins annotated to the listed GO biological terms found in all LPA-regulated or all identified phosphoproteins with annotated GO biological process terms.

For instance, the tumor suppressor protein programmed cell death protein 4 (PDCD4) was phosphorylated at Ser^{457}, a known Akt substrate site that regulates the repression of c-Jun-dependent transactivation of AP-1-responsive elements by PDCD4 (45). In addition, LPA induced phosphorylation on histone deacetylase 7 (HDAC7), likely through the upstream regulator PKD2, which has previously been characterized as cellular HDAC7 kinase and was activated in response to LPA as evident from increased activation loop phosphorylation (46). Notably, HDAC7 shuttles between the cytoplasm and the nucleus. Nuclear HDAC7 is recruited by the transcription factor MEF2D to its target gene promoters where it represses gene transcription. PKD-mediated phosphorylation leads to the accumulation of HDAC7 in the cytoplasm, thereby derepressing MEF2D/HDAC7-regulated genes (46–49). We observed LPA-induced HDAC7 phosphorylation on Ser^{486}, which has been functionally implicated in T cell receptor-mediated transcriptional regulation. By extension, our identification of Ser^{486} as an LPA-regulated phosphorylation site could indicate a similar role of HDAC7 in GPCR-mediated gene regulation. In addition to PKD2, also the closely related kinase PKD1 was linked to HDAC7 regulation, and both PKD1 and PKD2 are activated by LPA according to our data. Literature data suggest that PKD1 can be activated by bone morphogenic protein receptor 2 (BMPR2) (50) and that the serine/threonine kinase receptor BMPR2 undergoes autophosphorylation at Ser^{757} upon activation. Surprisingly, we found this particular phosphorylation site to be up-regulated by a factor of 2.6 upon LPA stimulation, pointing to a previously unknown cross-talk mechanism involving a transmembrane receptor with serine/threonine kinase activity as a potential mediator of transcriptional regulation through PKD and HDAC7. In addition, LPA rapidly induced phosphorylation of several other factors involved in protein biosynthesis, such as the transcription factor nuclear factor 1 X-type and the transcription elongation factor 3 as well as eukaryotic translation initiation factor 4H and Gem-associated protein 5 involved in protein translation.

The protein-protein interaction network of LPA-regulated phosphoproteins illustrates a remarkable gain in connectivity by the combined analysis of both kinase-enriched and total lysate fraction (Fig. 6). Data about regulated phosphoproteins were highly complementary, and only the protein kinases PKD1, calcium/calmodulin-dependent protein kinase type II δ, and calcium/calmodulin-dependent protein kinase kinase 1 were identified by either analytical strategy, whereas the majority of protein kinases identified in the LPA signaling response were contributed by the analysis of kinase inhibitor-resin-purified fractions.

Most protein kinases with LPA-induced phosphorylations are involved in either MAPK (TRAF2 and NCK-interacting kinase, TAO kinases 1/2, ERK1/2, and ribosomal protein S6 kinase α1/3), calcium-dependent (calcium/calmodulin-dependent protein kinases type II and PKDs), or tyrosine kinase signaling (Src, Yes, FAK, PYK2, and ABL1/2). It is noteworthy that several receptor tyrosine kinases such as Met, EGFR, and EPHB2 were phosphorylated at serine residues. These site-specific phosphorylations could influence their cellular activities and signaling capacities by, for example, modulating receptor trafficking and localization in conjunction

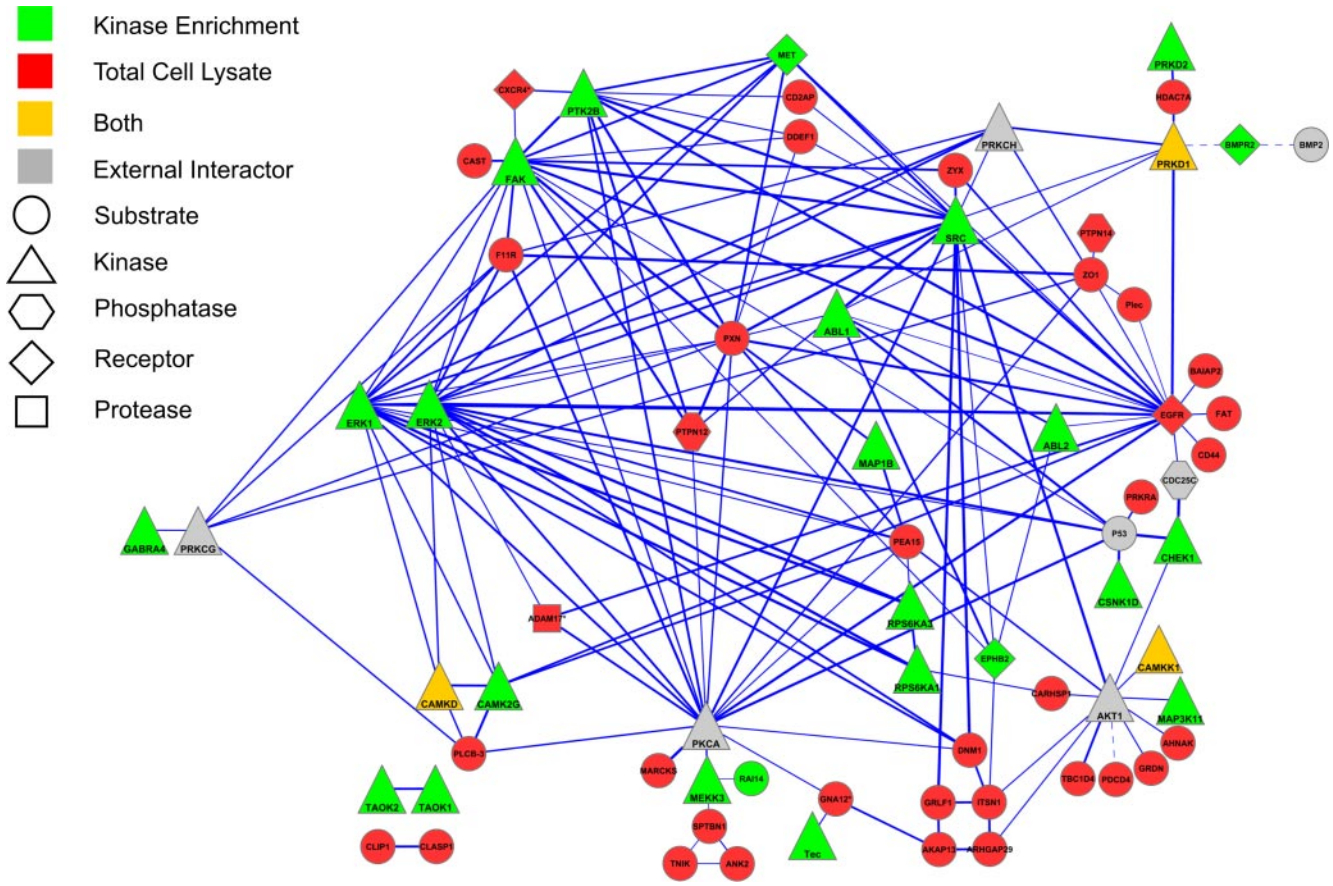

FIG. 6. **Network of LPA-regulated phosphoproteins.** Known physical and functional interactions among proteins with LPA-regulated phosphorylation sites were visualized using the STRING program. The *thickness* of the *edges* provides a measure for the confidence of the reported interactions according to the combination of experimental and database evidence. *Dashed edges* indicate interactions, which have been manually added to the STRING-generated network based on literature evidence. Gene names are displayed in the network that correspond to the following proteins: *ABL1*, proto-oncogene tyrosine-protein kinase ABL1; *ABL2*, tyrosine-protein kinase ABL2; *AHNAK*, neuroblast differentiation-associated protein AHNAK; *AKAP13*, protein kinase A anchor protein 13; *ANK2*, Ankyrin-2; *BAIAP2*, brain-specific angiogenesis inhibitor 1-associated protein 2; *BMP*, bone morphogenetic protein 1; *CAMKK1*, calcium/calmodulin-dependent protein kinase kinase 1; *CARHSP1*, calcium-regulated heat stable protein 1; *CAST*, calcium-binding protein CAST; *CAMKD*, calcium/calmodulin-dependent protein kinase II δ; *CAMK2G*, calcium/calmodulin-dependent protein kinase type II γ chain; *CDC25C*, M phase inducer phosphatase 3; *CD2AP*, CD2-associated protein; *CD44*, CD44 antigen; *CHEK1*, serine/threonine-protein kinase Chk1; *CLASP1*, CLIP-associating protein 1; *CLIP1*, CAP-Gly domain-containing linker protein 1; *CSNK1D*, casein kinase I isoform δ; *CXCR4*, CXC chemokine receptor type 4; *DDEF1*, 130-kDa phosphatidylinositol 4,5-bisphosphate-dependent ARF1 GTPase-activating protein; *DNM1*, dynamin-1; *EPHB2*, ephrin type-B receptor 2; *ERK1*, mitogen-activated protein kinase 3; *ERK2*, mitogen-activated protein kinase 1; *FAT*, protocadherin FAT-1; *F11R*, junctional adhesion molecule A; *GABRA4*, γ-aminobutyric acid receptor subunit α-4; *GNA12*, guanine nucleotide-binding protein subunit α-12; *GRDN*, girdin; *ITSN1*, intersectin-1; *MAP1B*, microtubule-associated protein 1B; *MARCKS*, myristoylated alanine-rich protein kinase C substrate; *MET*, hepatocyte growth factor receptor; *MEKK3*, mitogen-activated protein kinase kinase kinase 3; *PEA*, astrocytic phosphoprotein PEA15; *PLC3B*, 1-phosphatidylinositol-4,5-bisphosphate phosphodiesterase β-3; *PLEC*, plectin-1; *PRKD1*, serine/threonine-protein kinase D1; *PRKCG*, protein kinase C γ type; *PRKCH*, protein kinase C η type; *PRKRA*, interferon-inducible double-stranded RNA-dependent protein kinase activator A; *TK2B*, protein-tyrosine kinase 2β; *PTPN12*, protein-tyrosine phosphatase non-receptor type 12; *PTPN14*, protein-tyrosine phosphatase non-receptor type 14; *PXN*, paxillin; *RAI14*, ankycorbin; *RPS6KA1/3*, ribosomal protein S6 kinase α-1/3; *SPTBN1*, spectrin β chain, brain 1; *SRC*, proto-oncogene tyrosine-protein kinase Src; *TAOK1/2*, serine/threonine-protein kinase TAO-1/2; *TBC1D4*, TBC1 domain family member 4; *TEC*, tyrosine-protein kinase TEC; *TNIK*, TRAF2 and NCK-interacting protein kinase; *ZO1*, tight junction protein ZO-1; *ZYX*, zyxin.

with LPA-induced phosphorylations on several other factors implicated in endocytosis, such as AAK1, AP2 complex subunit β1, GTPase-activating protein and VPS9 domains 1, and dynamin 1.

Kinase Activation Loop Phosphorylations—Several LPA-induced phosphorylation events on protein kinases located to the conserved activation loop domain. As activation loop phosphorylation stabilizes the catalytically active conformation, these signaling events are of particular interest as they can provide a readout for cellular kinase activity. We found up-regulated activation loop phosphorylations on 11 distinct protein kinases (ERK1/2, FAK, PYK2, ribosomal protein S6

kinase α1, PKD1/2/3, Yes/Src, and Tec), indicating rapid induction of their catalytic activities upon LPA stimulation. Interestingly, the tyrosine kinase Tec plays an important role in diverse biological processes, such as antigen receptor signaling, actin reorganization, and cell adhesion (51). Tec might be of particular interest for further studies. Although Tec activation has been reported upon expression of either $G\alpha_{12/13}$ subunits or Src family kinases (52), our results provide the first evidence of Tec activation in the context of endogenous LPA signaling.

DISCUSSION

In our phosphoproteomics study, we analyzed early signaling events upon stimulation with the GPCR ligand LPA in comparison with HB-EGF treatment. HB-EGF was added at a concentration that induced EGFR tyrosine phosphorylation similar to that of the LPA-induced transactivation of the EGFR in A498 cells. Because of this experimental design, we could investigate how system-level effects, involving the EGFR and other components in LPA signaling, might affect downstream signal generation. Notably, nearly all HB-EGF-triggered phosphorylation events were more strongly induced by LPA. For example, LPA resulted in an about 2-fold stronger induction of activation loop phosphorylation in the MAP kinases ERK1 and ERK2, indicating synergism between EGFR transactivation and other branches of mitogenic LPA signaling. Although the underlying mechanisms are presently unclear, they could involve signal integration similar to the enhancement of EGF-triggered mitogenic signaling by insulin (53). Alternatively, LPA-induced phosphorylation changes might directly affect the signaling capacity of the EGFR, for example by modulation of its catalytic activity through site-specific serine/threonine phosphorylations on the receptor itself or by influencing its subcellular distribution through cross-talk to the endocytotic machinery. Interestingly, we found that LPA, but not HB-EGF, induced rapid phosphorylation events on several proteins with known functions in endocytosis, such as the serine/threonine kinase AAK1, dynamin 1, intersectin, GAPVD1, and AP2B1. Although the functional roles of these modifications remain to be determined, our study underlines the utility of quantitative phosphoproteomics to identify potential mechanisms of signal integration in growth factor signaling. Interestingly, we also detected strong LPA-induced phosphorylation on 7-dehydrocholesterol reductase (DHCR7), a metabolic enzyme involved in cholesterol biosynthesis. DHCR7 activity is positively regulated by phosphorylation (54), and depletion of cellular cholesterol increases ADAM17-mediated ligand shedding (55). Therefore, phosphorylation of DHCR7 may control a negative feedback loop that down-regulates ligand shedding in addition to effects on EGFR internalization due to increased membrane cholesterol levels (56).

The parallel phosphoproteomics analysis of total lysate and kinase-enriched fractions provided highly complementary information on phosphoproteins and their regulation as evident from the respective numbers of quantified phosphorylation sites. Overall, we quantified more than 10 times as many phosphopeptides as in a previous study on LPA signaling (57). Moreover, the merged information of kinases and kinase substrates proved to be essential for the generation of an LPA-regulated phosphoprotein network. The network connectivity was dramatically reduced in the case from kinase enrichment experiments were omitted. Therefore, our integrated phosphoproteomics approach is particularly useful for signal transduction analysis on the systems level as evident, for example, for protein kinases and other LPA-regulated phosphoproteins with roles in cell migration and adhesion. Network visualization with the STRING program revealed multiple associations of regulated phosphoproteins identified from total cell lysate, such as F11R, paxillin, and the protein-tyrosine phosphatase PTPN12, with protein kinases identified in the enrichment experiments, such as FAK, PYK2, Src, ERK MAP kinases, and others. In addition, LPA, but not HB-EGF, induced an about 3-fold up-regulation of $Ser(P)^{697}$ and $Ser(P)^{704}$ on the type I transmembrane glycoprotein CD44. Phosphorylation of Ser^{697} has been functionally linked to cell motility upon phorbol ester treatment (58). Furthermore, CD44 co-localizes and co-immunoprecipitates with the EGFR (59), which has also been implicated in LPA-triggered A498 cell migration and invasion (13). These lines of evidence point to a potential cooperation of CD44 and EGFR in LPA-induced migration, which might further involve a modulation of pro-HB-EGF processing by CD44 (60, 61). Collectively, this evidence together with our phosphoproteomics data and previous knowledge highlights the role of multifactorial signal processing within complex networks to modulate cell behavior such as a migratory response upon LPA stimulation. Such knowledge might be particularly relevant in the context of pathophysiological processes, such as cancer cell migration and invasion, and help to define cooperating signal factors for multitargeted therapeutic intervention to account for compensatory mechanisms in disease-relevant signaling networks.

Acknowledgments—We thank Axel Ullrich for the generous support of our work. We also gratefully acknowledge the continued support of Matthias Mann. We further thank Matthias Schneider for help and advice in the initial phase of this study and Renate Hornberger for excellent technical assistance.

* This work was supported by a grant from the Deutsche Forschungsgesellschaft.

S This article contains supplemental Figs. 1 and 2 and Tables 1–7.

** To whom correspondence should be addressed. Tel.: 49-89-8578-3773; Fax: 49-89-8578-2454; E-mail: daub@biochem.mpg.de.

REFERENCES

1. van Corven, E. J., Groenink, A., Jalink, K., Eichholtz, T., and Moolenaar, W. H. (1989) Lysophosphatidate-induced cell proliferation: identification and dissection of signaling pathways mediated by G proteins. *Cell* **59,** 45–54

2. Radeff-Huang, J., Seasholtz, T. M., Matteo, R. G., and Brown, J. H. (2004) G protein mediated signaling pathways in lysophospholipid induced cell proliferation and survival. *J. Cell. Biochem.* **92,** 949–966
3. Gardell, S. E., Dubin, A. E., and Chun, J. (2006) Emerging medicinal roles for lysophospholipid signaling. *Trends Mol. Med.* **12,** 65–75
4. Mills, G. B., and Moolenaar, W. H. (2003) The emerging role of lysophosphatidic acid in cancer. *Nat. Rev. Cancer* **3,** 582–591
5. van Meeteren, L. A., and Moolenaar, W. H. (2007) Regulation and biological activities of the autotaxin-LPA axis. *Prog. Lipid Res.* **46,** 145–160
6. Aoki, J., Inoue, A., and Okudaira, S. (2008) Two pathways for lysophosphatidic acid production. *Biochim. Biophys. Acta* **1781,** 513–518
7. Rozengurt, E. (2007) Mitogenic signaling pathways induced by G protein-coupled receptors. *J. Cell. Physiol.* **213,** 589–602
8. Ridley, A. J., and Hall, A. (1992) The small GTP-binding protein rho regulates the assembly of focal adhesions and actin stress fibers in response to growth factors. *Cell* **70,** 389–399
9. Hart, M. J., Jiang, X., Kozasa, T., Roscoe, W., Singer, W. D., Gilman, A. G., Sternweis, P. C., and Bollag, G. (1998) Direct stimulation of the guanine nucleotide exchange activity of p115 RhoGEF by Galpha13. *Science* **280,** 2112–2114
10. Yuan, J., Slice, L. W., Gu, J., and Rozengurt, E. (2003) Cooperation of Gq, Gi, and G12/13 in protein kinase D activation and phosphorylation induced by lysophosphatidic acid. *J. Biol. Chem.* **278,** 4882–4891
11. Daub, H., Wallasch, C., Lankenau, A., Herrlich, A., and Ullrich, A. (1997) Signal characteristics of G protein-transactivated EGF receptor. *EMBO J.* **16,** 7032–7044
12. Gohla, A., Harhammer, R., and Schultz, G. (1998) The G-protein G13 but not G12 mediates signaling from lysophosphatidic acid receptor via epidermal growth factor receptor to Rho. *J. Biol. Chem.* **273,** 4653–4659
13. Schäfer, B., Gschwind, A., and Ullrich, A. (2004) Multiple G-protein-coupled receptor signals converge on the epidermal growth factor receptor to promote migration and invasion. *Oncogene* **23,** 991–999
14. Fischer, O. M., Hart, S., Gschwind, A., and Ullrich, A. (2003) EGFR signal transactivation in cancer cells. *Biochem. Soc. Trans.* **31,** 1203–1208
15. Prenzel, N., Zwick, E., Daub, H., Leserer, M., Abraham, R., Wallasch, C., and Ullrich, A. (1999) EGF receptor transactivation by G-protein-coupled receptors requires metalloproteinase cleavage of proHB-EGF. *Nature* **402,** 884–888
16. Yan, Y., Shirakabe, K., and Werb, Z. (2002) The metalloprotease Kuzbanian (ADAM10) mediates the transactivation of EGF receptor by G protein-coupled receptors. *J. Cell Biol.* **158,** 221–226
17. Asakura, M., Kitakaze, M., Takashima, S., Liao, Y., Ishikura, F., Yoshinaka, T., Ohmoto, H., Node, K., Yoshino, K., Ishiguro, H., Asanuma, H., Sanada, S., Matsumura, Y., Takeda, H., Beppu, S., Tada, M., Hori, M., and Higashiyama, S. (2002) Cardiac hypertrophy is inhibited by antagonism of ADAM12 processing of HB-EGF: metalloproteinase inhibitors as a new therapy. *Nat. Med.* **8,** 35–40
18. Hart, S., Fischer, O. M., Prenzel, N., Zwick-Wallasch, E., Schneider, M., Hennighausen, L., and Ullrich, A. (2005) GPCR-induced migration of breast carcinoma cells depends on both EGFR signal transactivation and EGFR-independent pathways. *Biol. Chem.* **386,** 845–855
19. Mifune, M., Ohtsu, H., Suzuki, H., Nakashima, H., Brailoiu, E., Dun, N. J., Frank, G. D., Inagami, T., Higashiyama, S., Thomas, W. G., Eckhart, A. D., Dempsey, P. J., and Eguchi, S. (2005) G protein coupling and second messenger generation are indispensable for metalloprotease-dependent, heparin-binding epidermal growth factor shedding through angiotensin II type-1 receptor. *J. Biol. Chem.* **280,** 26592–26599
20. Pierce, K. L., Tohgo, A., Ahn, S., Field, M. E., Luttrell, L. M., and Lefkowitz, R. J. (2001) Epidermal growth factor (EGF) receptor-dependent ERK activation by G protein-coupled receptors: a co-culture system for identifying intermediates upstream and downstream of heparin-binding EGF shedding. *J. Biol. Chem.* **276,** 23155–23160
21. Zhang, Q., Thomas, S. M., Lui, V. W., Xi, S., Siegfried, J. M., Fan, H., Smithgall, T. E., Mills, G. B., and Grandis, J. R. (2006) Phosphorylation of TNF-alpha converting enzyme by gastrin-releasing peptide induces amphiregulin release and EGF receptor activation. *Proc. Natl. Acad. Sci. U.S.A.* **103,** 6901–6906
22. Mann, M. (2006) Functional and quantitative proteomics using SILAC. *Nat. Rev. Mol. Cell Biol.* **7,** 952–958
23. Larsen, M. R., Thingholm, T. E., Jensen, O. N., Roepstorff, P., and Jørgensen, T. J. (2005) Highly selective enrichment of phosphorylated peptides from peptide mixtures using titanium dioxide microcolumns. *Mol. Cell. Proteomics* **4,** 873–886
24. Olsen, J. V., Blagoev, B., Gnad, F., Macek, B., Kumar, C., Mortensen, P., and Mann, M. (2006) Global, in vivo, and site-specific phosphorylation dynamics in signaling networks. *Cell* **127,** 635–648
25. Olsen, J. V., de Godoy, L. M., Li, G., Macek, B., Mortensen, P., Pesch, R., Makarov, A., Lange, O., Horning, S., and Mann, M. (2005) Parts per million mass accuracy on an Orbitrap mass spectrometer via lock mass injection into a C-trap. *Mol. Cell. Proteomics* **4,** 2010–2021
26. Cox, J., and Mann, M. (2008) MaxQuant enables high peptide identification rates, individualized p.p.b.-range mass accuracies and proteome-wide protein quantification. *Nat. Biotechnol.* **26,** 1367–1372
27. Daub, H., Olsen, J. V., Bairlein, M., Gnad, F., Oppermann, F. S., Körner, R., Greff, Z., Kéri, G., Stemmann, O., and Mann, M. (2008) Kinase-selective enrichment enables quantitative phosphoproteomics of the kinome across the cell cycle. *Mol. Cell* **31,** 438–448
28. Wissing, J., Jänsch, L., Nimtz, M., Dieterich, G., Hornberger, R., Kéri, G., Wehland, J., and Daub, H. (2007) Proteomics analysis of protein kinases by target class-selective prefractionation and tandem mass spectrometry. *Mol. Cell. Proteomics* **6,** 537–547
29. Bantscheff, M., Eberhard, D., Abraham, Y., Bastuck, S., Boesche, M., Hobson, S., Mathieson, T., Perrin, J., Raida, M., Rau, C., Reader, V., Sweetman, G., Bauer, A., Bouwmeester, T., Hopf, C., Kruse, U., Neubauer, G., Ramsden, N., Rick, J., Kuster, B., and Drewes, G. (2007) Quantitative chemical proteomics reveals mechanisms of action of clinical ABL kinase inhibitors. *Nat. Biotechnol.* **25,** 1035–1044
30. Brehmer, D., Greff, Z., Godl, K., Blencke, S., Kurtenbach, A., Weber, M., Müller, S., Klebl, B., Cotten, M., Kéri, G., Wissing, J., and Daub, H. (2005) Cellular targets of gefitinib. *Cancer Res.* **65,** 379–382
31. Laird, A. D., Vajkoczy, P., Shawver, L. K., Thurnher, A., Liang, C., Mohammadi, M., Schlessinger, J., Ullrich, A., Hubbard, S. R., Blake, R. A., Fong, T. A., Strawn, L. M., Sun, L., Tang, C., Hawtin, R., Tang, F., Shenoy, N., Hirth, K. P., McMahon, G., and Cherrington, J. M. (2000) SU6668 is a potent antiangiogenic and antitumor agent that induces regression of established tumors. *Cancer Res.* **60,** 4152–4160
32. Shevchenko, A., Tomas, H., Havlis, J., Olsen, J. V., and Mann, M. (2006) In-gel digestion for mass spectrometric characterization of proteins and proteomes. *Nat. Protoc.* **1,** 2856–2860
33. Rappsilber, J., Mann, M., and Ishihama, Y. (2007) Protocol for micro-purification, enrichment, pre-fractionation and storage of peptides for proteomics using StageTips. *Nat. Protoc.* **2,** 1896–1906
34. Schroeder, M. J., Shabanowitz, J., Schwartz, J. C., Hunt, D. F., and Coon, J. J. (2004) A neutral loss activation method for improved phosphopeptide sequence analysis by quadrupole ion trap mass spectrometry. *Anal. Chem.* **76,** 3590–3598
35. Elias, J. E., Haas, W., Faherty, B. K., and Gygi, S. P. (2005) Comparative evaluation of mass spectrometry platforms used in large-scale proteomics investigations. *Nat. Methods* **2,** 667–675
36. Huang da, W., Sherman, B. T., Tan, Q., Collins, J. R., Alvord, W. G., Roayaei, J., Stephens, R., Baseler, M. W., Lane, H. C., and Lempicki, R. A. (2007) The DAVID Gene Functional Classification Tool: a novel biological module-centric algorithm to functionally analyze large gene lists. *Genome Biol.* **8,** R183
37. Jensen, L. J., Kuhn, M., Stark, M., Chaffron, S., Creevey, C., Muller, J., Doerks, T., Julien, P., Roth, A., Simonovic, M., Bork, P., and von Mering, C. (2009) STRING 8—a global view on proteins and their functional interactions in 630 organisms. *Nucleic Acids Res.* **37,** D412–D416
38. Cline, M. S., Smoot, M., Cerami, E., Kuchinsky, A., Landys, N., Workman, C., Christmas, R., Avila-Campilo, I., Creech, M., Gross, B., Hanspers, K., Isserlin, R., Kelley, R., Killcoyne, S., Lotia, S., Maere, S., Morris, J., Ono, K., Pavlovic, V., Pico, A. R., Vailaya, A., Wang, P. L., Adler, A., Conklin, B. R., Hood, L., Kuiper, M., Sander, C., Schmulevich, I., Schwikowski, B., Warner, G. J., Ideker, T., and Bader, G. D. (2007) Integration of biological networks and gene expression data using Cytoscape. *Nat. Protoc.* **2,** 2366–2382
39. Manning, G., Whyte, D. B., Martinez, R., Hunter, T., and Sudarsanam, S. (2002) The protein kinase complement of the human genome. *Science* **298,** 1912–1934
40. Zhang, W., Zheng, S., Storz, P., and Min, W. (2005) Protein kinase D specifically mediates apoptosis signal-regulating kinase 1-JNK signaling induced by H2O2 but not tumor necrosis factor. *J. Biol. Chem.* **280,**

19036–19044
41. Dutt, P., Nguyen, N., and Toksoz, D. (2004) Role of Lbc RhoGEF in Galpha12/13-induced signals to Rho GTPase. *Cell. Signal.* **16,** 201–209
42. Perfetti, A., Oriente, F., Iovino, S., Alberobello, A. T., Barbagallo, A. P., Esposito, I., Fiory, F., Teperino, R., Ungaro, P., Miele, C., Formisano, P., and Beguinot, F. (2007) Phorbol esters induce intracellular accumulation of the anti-apoptotic protein PED/PEA-15 by preventing ubiquitinylation and proteasomal degradation. *J. Biol. Chem.* **282,** 8648–8657
43. Trencia, A., Perfetti, A., Cassese, A., Vigliotta, G., Miele, C., Oriente, F., Santopietro, S., Giacco, F., Condorelli, G., Formisano, P., and Beguinot, F. (2003) Protein kinase B/Akt binds and phosphorylates PED/PEA-15, stabilizing its antiapoptotic action. *Mol. Cell. Biol.* **23,** 4511–4521
44. King, F. W., Skeen, J., Hay, N., and Shtivelman, E. (2004) Inhibition of Chk1 by activated PKB/Akt. *Cell Cycle* **3,** 634–637
45. Palamarchuk, A., Efanov, A., Maximov, V., Aqeilan, R. I., Croce, C. M., and Pekarsky, Y. (2005) Akt phosphorylates and regulates Pdcd4 tumor suppressor protein. *Cancer Res.* **65,** 11282–11286
46. Dequiedt, F., Van Lint, J., Lecomte, E., Van Duppen, V., Seufferlein, T., Vandenheede, J. R., Wattiez, R., and Kettmann, R. (2005) Phosphorylation of histone deacetylase 7 by protein kinase D mediates T cell receptor-induced Nur77 expression and apoptosis. *J. Exp. Med.* **201,** 793–804
47. Parra, M., Kasler, H., McKinsey, T. A., Olson, E. N., and Verdin, E. (2005) Protein kinase D1 phosphorylates HDAC7 and induces its nuclear export after T-cell receptor activation. *J. Biol. Chem.* **280,** 13762–13770
48. Dequiedt, F., Kasler, H., Fischle, W., Kiermer, V., Weinstein, M., Herndier, B. G., and Verdin, E. (2003) HDAC7, a thymus-specific class II histone deacetylase, regulates Nur77 transcription and TCR-mediated apoptosis. *Immunity* **18,** 687–698
49. Ishdorj, G., Graham, B. A., Hu, X., Chen, J., Johnston, J. B., Fang, X., and Gibson, S. B. (2008) Lysophosphatidic acid protects cancer cells from histone deacetylase (HDAC) inhibitor-induced apoptosis through activation of HDAC. *J. Biol. Chem.* **283,** 16818–16829
50. Jensen, E. D., Gopalakrishnan, R., and Westendorf, J. J. (2009) Bone morphogenic protein 2 activates protein kinase D to regulate histone deacetylase 7 localization and repression of Runx2. *J. Biol. Chem.* **284,** 2225–2234
51. Takesono, A., Horai, R., Mandai, M., Dombroski, D., and Schwartzberg, P. L. (2004) Requirement for Tec kinases in chemokine-induced migration and activation of Cdc42 and Rac. *Curr. Biol.* **14,** 917–922
52. Mao, J., Xie, W., Yuan, H., Simon, M. I., Mano, H., and Wu, D. (1998) Tec/Bmx non-receptor tyrosine kinases are involved in regulation of Rho and serum response factor by Galpha12/13. *EMBO J.* **17,** 5638–5646
53. Borisov, N., Aksamitiene, E., Kiyatkin, A., Legewie, S., Berkhout, J., Maiwald, T., Kaimachnikov, N. P., Timmer, J., Hoek, J. B., and Kholodenko, B. N. (2009) Systems-level interactions between insulin-EGF networks amplify mitogenic signaling. *Mol. Syst. Biol.* **5,** 256
54. Shefer, S., Salen, G., Honda, A., Batta, A. K., Nguyen, L. B., Tint, G. S., Ioannou, Y. A., and Desnick, R. (1998) Regulation of rat hepatic 3beta-hydroxysterol delta7-reductase: substrate specificity, competitive and non-competitive inhibition, and phosphorylation/dephosphorylation. *J. Lipid Res.* **39,** 2471–2476
55. von Tresckow, B., Kallen, K. J., von Strandmann, E. P., Borchmann, P., Lange, H., Engert, A., and Hansen, H. P. (2004) Depletion of cellular cholesterol and lipid rafts increases shedding of CD30. *J. Immunol.* **172,** 4324–4331
56. Lambert, S., Ameels, H., Gniadecki, R., Hérin, M., and Poumay, Y. (2008) Internalization of EGF receptor following lipid rafts disruption in keratinocytes is delayed and dependent on p38 MAPK activation. *J. Cell. Physiol.* **217,** 834–845
57. Ding, S. J., Wang, Y., Jacobs, J. M., Qian, W. J., Yang, F., Tolmachev, A. V., Du, X., Wang, W., Moore, R. J., Monroe, M. E., Purvine, S. O., Waters, K., Heibeck, T. H., Adkins, J. N., Camp, D. G., 2nd, Klemke, R. L., and Smith, R. D. (2008) Quantitative phosphoproteome analysis of lysophosphatidic acid induced chemotaxis applying dual-step (18)O labeling coupled with immobilized metal-ion affinity chromatography. *J. Proteome Res.* **7,** 4215–4224
58. Tzircotis, G., Thorne, R. F., and Isacke, C. M. (2006) Directional sensing of a phorbol ester gradient requires CD44 and is regulated by CD44 phosphorylation. *Oncogene* **25,** 7401–7410
59. Wobus, M., Rangwala, R., Sheyn, I., Hennigan, R., Coila, B., Lower, E. E., Yassin, R. S., and Sherman, L. S. (2002) CD44 associates with EGFR and erbB2 in metastasizing mammary carcinoma cells. *Appl. Immunohistochem. Mol. Morphol.* **10,** 34–39
60. Nagano, O., Murakami, D., Hartmann, D., De Strooper, B., Saftig, P., Iwatsubo, T., Nakajima, M., Shinohara, M., and Saya, H. (2004) Cell-matrix interaction via CD44 is independently regulated by different metalloproteinases activated in response to extracellular Ca(2+) influx and PKC activation. *J. Cell Biol.* **165,** 893–902
61. Stoeck, A., Keller, S., Riedle, S., Sanderson, M. P., Runz, S., Le Naour, F., Gutwein, P., Ludwig, A., Rubinstein, E., and Altevogt, P. (2006) A role for exosomes in the constitutive and stimulus-induced ectodomain cleavage of L1 and CD44. *Biochem. J.* **393,** 609–618
62. Aoki, N., Ueno, S., Mano, H., Yamasaki, S., Shiota, M., Miyazaki, H., Yamaguchi-Aoki, Y., Matsuda, T., and Ullrich, A. (2004) Mutual regulation of protein-tyrosine phosphatase 20 and protein-tyrosine kinase Tec activities by tyrosine phosphorylation and dephosphorylation. *J. Biol. Chem.* **279,** 10765–10775
63. Sabourin, L. A., Tamai, K., Seale, P., Wagner, J., and Rudnicki, M. A. (2000) Caspase 3 cleavage of the Ste20-related kinase SLK releases and activates an apoptosis-inducing kinase domain and an actin-disassembling region. *Mol. Cell. Biol.* **20,** 684–696
64. Zhang, X., Orlando, K., He, B., Xi, F., Zhang, J., Zajac, A., and Guo, W. (2008) Membrane association and functional regulation of Sec3 by phospholipids and Cdc42. *J. Cell Biol.* **180,** 145–158
65. Fierro-Monti, I., Mohammed, S., Matthiesen, R., Santoro, R., Burns, J. S., Williams, D. J., Proud, C. G., Kassem, M., Jensen, O. N., and Roepstorff, P. (2006) Quantitative proteomics identifies Gemin5, a scaffolding protein involved in ribonucleoprotein assembly, as a novel partner for eukaryotic initiation factor 4E. *J. Proteome Res.* **5,** 1367–1378
66. Yan, D., and Olkkonen, V. M. (2008) Characteristics of oxysterol binding proteins. *Int. Rev. Cytol.* **265,** 253–285